Ocean Sci. Discuss., https://doi.org/10.5194/os-2018-11
Manuscript under review for journal Ocean Sci.
Discussion started: 20 February 2018

Numerical modeling of surface wave development under the action of wind

DMITRY CHALIKOV
Shirshov Institute of Oceanology, Saint Petersburg 199053, Russia
Russian State Hydrometeorological University, SaintPetersburg195196
University of Melbourne, Victoria 3010, Australia

Abstract

The numerical modeling of two-dimensional surface wave development under the action of wind is performed. The model is based on three-dimensional equations of potential motion with free surface written in a surface-following non-orthogonal curvilinear coordinate system where depth is counted from moving surface. Three-dimensional Poisson equation for velocity potential is solved iteratively. Fourier transform method, the second-order accuracy approximation of vertical derivatives on a stretched vertical grid and the fourth-order Runge-Kutta time stepping are used. Both the input energy to waves and dissipation of wave energy are calculated on the basis of the earlier developed and validated algorithms. A one-processor version of the model for PC allows us to simulate an evolution of wave field with thousands degrees of freedom over thousands of wave periods. A long-time evolution of two-dimensional wave structure is illustrated by the spectra of wave surface and input and output of energy.

1. Introduction

Development of waves under the action of wind is a process that is difficult to simulate since surface waves are very conservative and change their energy for hundreds and thousands periods. This is why the most popular method is spectral modeling. Waves as physical objects in this approach are actually absent, since evolution of spectral distribution of wave energy is simulated. The description of input and dissipation in this approach is not connected directly with the formulation of the problem, but it is rather adopted from other branches of wave theory where waves are the objects of investigation. However, the spectral approach turned out to be the only method capable to describe the space and time evolution of wave field in the ocean. The phase resolving models (or 'direct' models) designed for reproducing waves themselves cannot compete with spectral models since a typical size of domain in such models does not exceed several kilometers. Such domain includes just several thousands of large waves. Nevertheless, direct wave modeling plays an ever-increasing role in geophysical fluid dynamics, because it gives the possibility to investigate the processes which cannot be reproduced with spectral models. One of such problems is that of extreme wave generation. (Chalikov, 2009; Chalikov, Babanin, 2016a).Direct modeling is also a perfect instrument for development of parameterization of physical processes for spectral wave models. Besides, such models can be used for direct simulation of wave regimes of small water basins, for example, port harbors. Other approaches of direct modeling are discussed in (Chalikov et al. 2014; Chalikov, 2016)

Until recently, direct modeling was used for reproduction of quasi-stationary wave regime when wave spectrum essentially did not change. A unique example of direct numerical modeling of surface wave evolution is given in (Chalikov and Babanin, 2014)where development of wave field was calculated with use of a two-dimensional model based on full

Ocean Sci. Discuss., https://doi.org/10.5194/os-2018-11
Manuscript under review for journal Ocean Sci.
Discussion started: 20 February 2018

potential equations written in the conformal coordinates. The model included algorithms for parameterization of input and dissipation of energy (a description of similar algorithms is given below). The model successfully reproduced an evolution of wave spectrum under the action of wind. However, strictly one-dimensional (unidirected) waves are not realistic; hence, the full problem of wave evolution should be formulated on the basis of three-dimensional equations. An example of such modeling is given in the current paper.

2. Equations

Let us introduce a *non-stationary surface-following non-orthogonal* coordinate system:

$$\xi = x, \quad \vartheta = y, \quad \zeta = z - \eta(\xi, \vartheta, \tau), \quad \tau = t\,, \tag{1}$$

where $\eta(x, y, t) = \eta(\xi, \vartheta, \tau)$ is a moving periodic wave surface given by the Fourier series

$$\eta(\xi, \vartheta, \tau) = \sum_{-M_x<k<M_x} \sum_{-M_y<l<M_y} h_{k,l}(\tau)\Theta_{k,l}\,, \tag{2}$$

where M_x and M_y are the numbers of modes in directions ξ and ϑ, respectively, while $\Theta_{k,l}$ are Fourier expansion basis functions. The 3-D equations of potential waves in the system of coordinates (1) at $\zeta \le 0$ take the following form:

$$\eta_\tau = -\eta_\xi \varphi_\xi - \eta_\vartheta \varphi_\vartheta + \left(1 + \eta_\xi^2 + \eta_\vartheta^2\right)\Phi_\varsigma\,, \tag{3}$$

$$\varphi_\tau = -\frac{1}{2}\left(\varphi_\xi^2 + \varphi_\vartheta^2 - \left(1 + \eta_\xi^2 + \eta_\vartheta^2\right)\Phi_\zeta^2\right) - \eta - p\,, \tag{4}$$

$$\Phi_{\xi\xi} + \Phi_{\vartheta\vartheta} + \Phi_{\zeta\zeta} = \Upsilon(\Phi)\,, \tag{5}$$

where Υ is the operator:

$$\Upsilon() = 2\eta_\xi()_{\xi\zeta} + 2\eta_\vartheta()_{\vartheta\zeta} + \left(\eta_{\xi\xi} + \eta_{\vartheta\vartheta}\right)()_\zeta - \left(\eta_\xi^2 + \eta_\vartheta^2\right)()_{\zeta\zeta}\,, \tag{6}$$

capital fonts Φ are used for domain $\zeta < 0$ while the lower case φ refers to $\zeta = 0$.

It is suggested in (Chalikov et al., 2014) that it is convenient to represent velocity potential φ as a sum of two components, i.e., an analytical ('linear') component $\bar{\Phi}, \left(\bar{\varphi} = \bar{\Phi}(\xi, \vartheta, 0)\right)$ and an arbitrary ('non-linear') component $\tilde{\Phi}, \left(\tilde{\varphi} = \tilde{\Phi}(x, y, 0)\right)$:

$$\varphi = \bar{\varphi} + \tilde{\varphi}, \quad \Phi = \bar{\Phi} + \tilde{\Phi}\,. \tag{7}$$

The analytical component $\bar{\Phi}$ satisfies Laplace equation:

$$\bar{\Phi}_{\xi\xi} + \bar{\Phi}_{\vartheta\vartheta} + \bar{\Phi}_{\zeta\zeta} = 0\,, \tag{8}$$

with known solution:

$$\bar{\Phi}(\xi, \vartheta, \zeta) = \sum_{k,l} \bar{\varphi}_{k,l} \exp\left(|k|\zeta\right)\Theta_{k,l}\,, \tag{9}$$

($\bar{\varphi}_{k,l}$ are Fourier coefficients of surface analytical potential $\bar{\varphi}$ at $\zeta = 0$). The solution satisfies boundary conditions:

$$\begin{aligned} &\varsigma = 0: \quad \bar{\Phi} = \bar{\varphi} \\ &\varsigma \to -\infty: \quad \tilde{\Phi}_\zeta \to 0 \end{aligned} \tag{10}$$

The nonlinear component satisfies an equation:

Ocean Sci. Discuss., https://doi.org/10.5194/os-2018-11
Manuscript under review for journal Ocean Sci.
Discussion started: 20 February 2018

$$\tilde{\Phi}_{\xi\xi} + \tilde{\Phi}_{\vartheta\vartheta} + \tilde{\Phi}_{\zeta\zeta} = \Upsilon\left(\tilde{\Phi}\right) + \Upsilon\left(\bar{\Phi}\right), \tag{11}$$

Eq. (11) is solved with the boundary conditions:

$$\begin{aligned} &\varsigma = 0: \quad \tilde{\Phi} = 0 \\ &\varsigma \to -\infty: \quad \tilde{\Phi}_{\varsigma} \to 0 \end{aligned} \tag{12}$$

The derivatives of linear component $\bar{\Phi}$ in (6) are calculated analytically. The scheme combines 2-D Fourier transform method in the 'horizontal surfaces' and a second-order finite-difference approximation on a stretched staggered grid defined by relation $\Delta\zeta_{j+1} = \chi\Delta\zeta_j$ ($\Delta\zeta$ is a vertical step, while $j = 1$ at the surface). The stretched grid provides increase of accuracy of approximation for the exponentially decaying modes. The values of stretching coefficient χ lie within the interval 1.01-1.20. A finite-difference second-order approximation of Eq. (10) on a non-uniform vertical grid is quite straightforward. Equation (11) is solved as Poisson equations with iterations over the right-hand side. A detailed description of the scheme and its validation is given in (Chalikov, 2016).

Equations (3) – (5) are written in a non-dimensional form by using the following scales: length L where $2\pi L$ is (dimensional) period in the horizontal direction; time $L^{1/2}g^{-1/2}$ and velocity potential $L^{3/2}g^{1/2}$ (g is acceleration of gravity). The pressure is normalized by water density, so that the pressure scale is Lg. Equations (3) – (5) are self-similar to the transformation with respect to L. All the results presented in this paper are nondimensional.

3. Energy input and dissipation

Input energy to waves describes a pressure term p in a dynamic boundary condition (4). Dissipation cannot be described with use of potential equations, but for realistic description of wave dynamics, dissipation of wave energy should be taken into account, i.e., we should include in equations (3) and (4) additional terms which, strictly speaking, contradict the assumption of potentiality.

3.1 Energy input from wind

According to the linear theory(Miles, 1957), the Fourier components of surface pressure p are connected with those of surface elevation through the following expression:

$$p_{k,l} + \mathrm{i}p_{-k,-l} = \frac{\rho_a}{\rho_w}\left(\beta_{k,l} + \mathrm{i}\beta_{-k,-l}\right)\left(h_{k,l} + \mathrm{i}h_{-k,-l}\right), \tag{13}$$

where $h_{k,l}, h_{-k,-l}, \beta_{k,l}, \beta_{-k,-l}$, are real and imaginary parts of elevation η and the so-called β-function (i.e., Fourier coefficients at COS and SIN, respectively); ρ_a / ρ_w is a ratio of air and water densities, respectively. Hence, for derivation of shape of beta-function it is necessary to simultaneously measure wave surface elevation and non-static pressure on the surface. Experimental measurement of surface pressure is a very difficult problem since the measurements should be done very close to a moving surface, preferably, with a surface-following sensor. Such measurements are done quite seldom, especially, in the field. The measurements were carried out for the first time by a team of authors both in laboratory and field (Snyder et al, 1981; Hsiao and Shemdin, 1983; Hasselmann and Bösenberg, 1991; Donelan et al., 2005, 2006). The data obtained in this way allowed constructing an imaginary part of beta-

Ocean Sci. Discuss., https://doi.org/10.5194/os-2018-11
Manuscript under review for journal Ocean Sci.
Discussion started: 20 February 2018

function used in some versions of wave forecasting models (Rogers et al. 2012). The second way of beta-function evaluation is based on the results of numerical investigations of statistical structure of the boundary layer above waves with use of Reynolds equations and an appropriate closure scheme. In general, this method works so well that many problems in the technical fluid mechanics are often solved using numerical models, not experimentally. This method was being developed beginning from (Chalikov, 1978, 1986), followed by (Chalikov and Makin, 1991; Chalikov and Belevich, 1992; Chalikov, 1995). The results were implemented in WAVEWATCH model, i.e., a third-generation wave forecast model (Tolman and Chalikov, 1996) and thoroughly validated against the experimental data in the course of developing WAVEWATCH-III (Tolman et al., 2014). This method was later improved on the basis of more advanced coupled modeling of waves and boundary layer (Chalikov and Rainchk, 2010; hereafter CR), while the beta-function used in WAVEWATCH-III was corrected and extended up to high frequencies. Direct calculation of energy input to waves requires both real and imaginary parts of the beta-function. The total energy input to waves depends on imaginary part of β -function, while the moments of higher order depend both on imaginary and real parts of β . This is why full approximation constructed in CR was used in the current work. Note that in the range of relatively low frequencies the new method is very close to the scheme implemented in WAVEWATCH-III.

It is a traditional suggestion that both coefficients are the functions of virtual nondimensional frequency $\Omega = \omega_k U \cos\psi = U / c_k \cos\psi$ (where ω_k and U are the nondimensional radian frequency and wind speed, respectively; c_k is a phase speed of the kth mode; ψ is an angle between wind and wave mode directions). Most of the schemes for calculations of β-function consider a relatively narrow interval of nondimensional frequencies Ω. In the current work, the range of frequencies covers an interval $\left(0 < \Omega_p < 10\right)$, and occasionally the values of $\Omega > 10$ can appear. This is why the function derived in (Chalikov and Rainchik, 2010) through coupled simulations of waves and boundary layer, is used here. Wave model is based on potential equations for a flow with free surface, extended with an algorithm for breaking dissipation (see below description of the breaking dissipation parameterization). Wave boundary layer (WBL) model is based on Reynolds equations closed with $K-\varepsilon$ scheme; solutions for air and water are matched through the interface. The β-function obtained in CR was used for evaluation of accuracy of the surface pressure p calculations. A shape of β-function connecting surface elevations and surface pressure, is studied up to high nondimensional wave frequencies both in positive and negative (i.e., for wind opposite to waves) domains. The data on β-function exhibit wide scatter, but since the volume of data was quite large (47 long-term numerical runs allowed us to generate about 1,400,000 values of β), the shape of β-function was defined with satisfactory accuracy up to very high nondimensional frequencies $\left(-50 < \Omega < 50\right)$. As a result, the data on β-function in such a broad range, allow us to calculate wave drag up to very high frequencies and to explicitly divide the fluxes of energy and momentum transferred by the pressure and molecular viscosity. This method is free of arbitrary assumptions on the drag coefficient C_d; and, on the contrary, such calculations allow investigating the nature of wave drag (see Ting et al., 2012)

It was indicated above that an initial wave field is assigned as superposition of linear modes which amplitudes are calculated with JONSWAP spectrum with peak wave number

Ocean Sci. Discuss., https://doi.org/10.5194/os-2018-11
Manuscript under review for journal Ocean Sci.
Discussion started: 20 February 2018

$k_p = 100$.The initial value $\Omega_0 = 6$ was chosen, i.e.,a ratio of the nondimensional wind speed at height $\lambda_0 / 2 = 2\pi / 100$ and the phase speed $c_0 = k_0^{-1/2}$ is equal to 6. Such a high ratio corresponds to initial stages of wave development. The values of Ω for other wave numbers are calculated by assuming that wind profile is logarithmic:

$$\Omega_k = \Omega_0 \frac{c_0}{c_k} \ln \frac{\lambda_k}{2z_0} \left(\ln \frac{\lambda_0}{2z_{00}} \right)^{-1} \cos\psi \,, \tag{14}$$

where z_{00} is effective nondimensional roughness for the initial wind profile, while z_0 is the actual roughness parameter that depends on the energy in a high-frequency part of spectrum and on the wind profile. We call it 'effective', since very close to the surface the wind profile is not logarithmic (Chalikov, 1995; Tolman, Chalikov, CR). The value of this parameter depends on the wind velocity and energy in a high-wave number interval of wave spectrum, as well as on the length scale of the problem. All these effects are possible to include by matching the wave model with a one dimensional WBL model(Ting et al, 2012). Here, a simplified scheme for the roughness parameter is chosen. It is well known that the roughness parameter (as well as a drag coefficient) decreases with decrease of the inverse wave age. In our case wind speed is fixed, and dependence for the nondimensional roughness parameter is constructed on the basis of the results obtained in CR:

$$z_0 = 15 z_{00} \Omega \,, \tag{15}$$

where $z_{00} = 10^{-3}$ is the initial value of the roughness parameter. Eq. (15) approximates dependence of the effective roughness at the stage of wave development. Note that the results are not sensitive to variation of the roughness parameter within reasonable limits.

3.2 High wave number energy dissipation

A nonlinear flux of energy directed to the small wave numbers produces downshifting of spectrum, while an opposite flux forms a shape of spectral tail. The second process can produce accumulation of energy near 'cut' wave number. Both processes become more intensive with increase of energy input. Growth of amplitudes at high wave numbers is followed by the growth of local steepness and numerical instability. This phenomenon well known in numerical fluid mechanics is eliminated by use of a highly selective filter simulating nonlinear viscosity. To support stability, additional terms are included into the right hand sides of equations (3) and (4):

$$\frac{\partial \eta_{k,l}}{\partial \tau} = E_{k,l} - \mu_{k,l} \eta_{k,l} \,, \tag{16}$$

$$\frac{\partial \varphi_{k,l}}{\partial \tau} = F_{k,l} - \mu_{k,l} \varphi_{k,l} \tag{17}$$

($E_{k,l}$ and $F_{k,l}$ are Fourier amplitudes of the right-hand sides of equations (3) and (4) while factor $\mu_{k,l}$ is calculated using a formula:

Ocean Sci. Discuss., https://doi.org/10.5194/os-2018-11
Manuscript under review for journal Ocean Sci.
Discussion started: 20 February 2018

$$\mu_{k,l} = \begin{cases} 0 & |k| < k_d \\ c_m k_0 \left(\dfrac{|k| - k_d}{(k_0 - k_d)} \right)^2 & k_d \le |k| \le k_0 \\ c_m k_0 & |k| > k_0 \end{cases} \tag{18}$$

where k and l are components of wave number $|k|$, while coefficients k_d and k_0 are defined by the expressions:

$$k_d = d_m^2 M_x M_y \left(\left(l |k|^{-1} d_m M_x \right)^2 + \left(k |k|^{-1} d_m M_y \right)^2 \right)^{-1/2} \tag{19}$$

$$k_0 = M_x M_y \left(\left(l |k|^{-1} M_x \right)^2 + \left(k |k|^{-1} M_y \right)^2 \right)^{-1/2} \tag{20}$$

where $c_m = 0.1, d_m = 0.75$. Expressions (18) - (20) can be interpreted in a straightforward way: the value of $\mu_{k,l}$ is equal to zero inside the ellipse with semi-axes $d_m M_x$ and $d_m M_y$; then it grows linearly with $|k|$ up to the value c_m and is equal to c_m outside the outer ellipse. This method of filtration that we call 'tail dissipation' was developed and validated with a conformal model by Chalikov and Sheinin (1998). The sensitivity of the results to the parameters in (18) - (20) is not high. The aim of the algorithm is support of smoothness and monotonicity of wave spectrum within a high wave number range. Since the algorithm affects amplitudes of small modes, it actually does not reduce the total energy, though it efficiently prevents development of numerical instability. Note that any long-term calculations cannot be performed without 'tail dissipation' eliminating development of the numerical instability at high wave numbers.

3.3 Dissipation due to wave breaking

The main process of wave dissipation is wave breaking. This process is taken into account in all spectral wave forecasting models similar to WAVEWATCH (see Tolman and Chalikov, 1996).Since there are no waves in spectral models, no local criteria of wave breaking can be formulated. This is why breaking dissipation is represented in spectral models in a distorted form. Areal breaking occurs in relatively narrow areas of physical space; however, spectral image of such breaking is stretched over the entire wave spectrum, while in reality the breaking decreases height and energy of dominant waves. This contradiction occurs because waves in spectral models are assumed as linear ones, while in fact the breaking occurs in physical space with nonlinear sharp wave, usually composed of several modes.

The mechanics of wave breaking at developed wave spectrum differs from that in a wave field represented by few modes, normally considered in many theoretical and laboratory investigations. Since the breaking in laboratory conditions is initiated by special assigning of amplitudes and phases, it cannot be similar to the breaking in natural conditions. To some degree, the wave breaking is similar to development of extreme wave that appears suddenly with no pronounced prehistory (Chalikov and Babanin, 2016a, 2016b). There are no signs of modulational instability in both phenomena, which suggests a process of taking energy from other modes. The evolution leading to breaking or 'freaking' seems just opposite: full energy of main wave remains nearly constant while the columnar energy is focusing around the crest of this wave which becomes sharper and unstable. Probably, even more frequent cases of wave

Ocean Sci. Discuss., https://doi.org/10.5194/os-2018-11
Manuscript under review for journal Ocean Sci.
Discussion started: 20 February 2018

breaking and extreme wave appearance can be explained by local superposition of several modes.

The instability of interface leading to breaking is an important and poorly developed problem of fluid mechanics. In general, this essentially nonlinear process should be investigated for a two-phase flow. Such approach was demonstrated, for example, by Iafrati (2001). However, the progress in solving this highly complicated problem is not too fast.

The problem of breaking parameterization includes two points: (1) establishing of a criterion of breaking onset and (2) developing of an algorithm of breaking parameterization. The problem of breaking is discussed in details in Babanin (2011). Chalikov and Babanin (2012) performed numerical investigation of the processes leading to breaking. It was found that a clear predictor of breaking, formulated in dynamical and geometrical terms, probably does not exist. The most evident criterion of breaking is the breaking itself, i.e., the process when some part of upper portion of sharp wave crest is falling down. This process is usually followed by separation of detached volume of liquid into water and air phases. Unfortunately, there is no possibility to describe this process within the scope of potential theory.

Some investigators suggest using the physical velocity approaching the rate of surface movement in the same direction as a criterion of breaking onset. This is incorrect, since the kinematic boundary condition suggests that these quantities are exactly equal to each other. It is quite clear that the onset of breaking can be characterized by appearance of non-single-value piece of surface. This stage can be investigated with two-dimensional model which due to a high flexibility of the conformal coordinates allows us to reproduce a surface with the inclination in the Cartesian coordinates larger than 90 degrees. (In the conformal coordinates the dependence of elevation on curvilinear coordinate is always single-value). The duration of this stage is extremely short, the calculations being always interrupted by the numerical instability with sharp violation of conservations laws (constant integral invariants, i.e., full energy and volume) and strong distortion of the local structure of flow. Numerous numerical experiments with conformal model showed that after appearance of non-single value, the model never returns to stability. However, introducing of appearance of the non-single-surface as a criterion of breaking instability even in conformal model is impossible, since a behavior of model at a critical point is unpredictable, and the run is most likely to be terminated, no matter what kind of parameterization of breaking is introduced. It means that even in a very precise conformal model, stabilization of solution should be initiated prior to breaking.

Consideration of exact criterion for breaking onset for the models using transformation of the coordinate type (1) is useless, since the numerical instability in such models arises not because of the breaking approaching but because of appearance of large local steepness. Multiple experiments with direct 3-D wave model show that appearance of local steepness $\max\left(\partial\eta/\partial x, \partial\eta/\partial y\right)$ exceeding ≈ 2 (that corresponds to a slope of about 60 degrees) is always followed by numerical instability. Decrease of time step does not make any effect. As seen, a surface with such slope is very far from being a vertical ‘wall’, when real breaking starts. However, an algorithm for breaking parameterization must prevent appearance of large local steepness. The situation is similar to the numerical modeling of turbulence (LES technique), where the local highly selective viscosity is used to prevent appearance of too large local gradients of velocity. The description of breaking in direct wave modeling should satisfy the following conditions. (1) It should prevent large local gradients of elevation; in our case the

Ocean Sci. Discuss., https://doi.org/10.5194/os-2018-11
Manuscript under review for journal Ocean Sci.
Discussion started: 20 February 2018

breaking algorithm should prevent the onset of instability at each point of half million of grid points over more than 100 thousand of time steps.(2) It should describe in a more or less realistic way the loss of kinetic and potential energies with preservation of balance between them. (3) It should preserve the volume. It was suggested in (Chalikov, 2005) that an acceptable scheme can be based on the local highly selective diffusion operator with special diffusion coefficient. Several schemes of such type were validated, and finally the following scheme was chosen:

$$\eta_\tau = E_\eta + J^{-1}\left(\frac{\partial}{\partial\xi}B_\xi\frac{\partial\eta}{\partial\xi}+\frac{\partial}{\partial\vartheta}B_\vartheta\frac{\partial\eta}{\partial\vartheta}\right), \tag{21}$$

$$\varphi_\tau = F_\varphi + J^{-1}\left(\frac{\partial}{\partial\xi}B_\xi\frac{\partial\varphi}{\partial\xi}+\frac{\partial}{\partial\vartheta}B_\vartheta\frac{\partial\varphi}{\partial\vartheta}\right), \tag{22}$$

where F_η and F_φ are the right-hand sides of equations (3) and (4) including the terms introduced by (16) – (20). It was suggested in the first versions of the scheme that diffusion coefficient depends on a local slope, however, such scheme did not prove to be very reliable since it did not prevent all of the events of numerical instability. A scheme based on the calculation of the local curvilinearity $\eta_{\xi\xi}$ and $\eta_{\vartheta\vartheta}$ turned out to be a lot more reliable. The calculations of 75 different runs were performed with full 3-D model in (Chalikov et al, 2014) over period of $t = 350$ (70,000 time steps). The total number of values used for the calculations of dependence in Fig. 1 (thick curve) is about 6 billion. The normal probability calculated with the same dispersion is shown by thin curve.

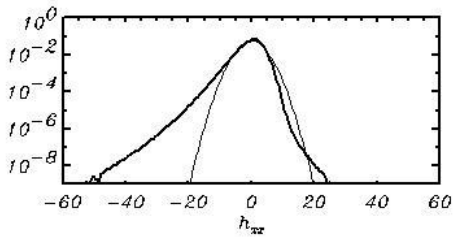

Figure 1. Probability of curvilinearity $\eta_{\xi\xi}$. Thick curve calculated with full 3-D model; thin curve is a probability calculated over ensemble of linear modes with the same spectrum.

It is seen that the probability of large negative values of curvilinearity is by orders larger than the probability calculated over ensemble of linear modes with the same spectrum.

The curvilinearity turned out to be very sensitive to the shape of surface. This is why it was chosen as a criterion of breaking approach. Coefficients B_ξ and B_ϑ depend nonlinearly on the curvilinearity

$$B_\xi = \begin{cases} \Delta\xi C_B \eta_{\xi\xi}^2 & \eta_{\xi\xi} < \eta_{\xi\xi}^{cr} \\ 0 & \eta_{\xi\xi} \geq \eta_{\xi\xi}^{cr} \end{cases} \tag{23}$$

$$B_\vartheta = \begin{cases} \Delta\vartheta C_B \eta_{\vartheta\vartheta}^2 & \eta_{\vartheta\vartheta} < \eta_{\xi\xi}^{cr} \\ 0 & \eta_{\vartheta\vartheta} \geq \eta_{\xi\xi}^{cr} \end{cases} \tag{24}$$

where $\Delta\xi$ and $\Delta\zeta$ are horizontal steps in *x* and *y* direction in grid space, and coefficients are $C_B = 2.0$, $\eta_{\xi\xi}^{cr} = \eta_{\vartheta\vartheta}^{cr} = -50$. Algorithm (21) - (24) does not change the volume and decreases the local potential and kinetic energy. It is assumed that the lost momentum and energy are

Ocean Sci. Discuss., https://doi.org/10.5194/os-2018-11
Manuscript under review for journal Ocean Sci.
Discussion started: 20 February 2018

transferred to current and turbulence (see Chalikov and Belevich, 1992). Besides, the energy also goes to other wave modes. The choice of parameters in (21) - (24) is based on simple considerations: local piece of surface can closely approach the critical curvilinearity but not exceed it. The values of the coefficients are picked with reserve to provide stability of long runs.

We do not think that the suggested breaking parameterization is a final solution of the problem. Other schemes will be tried in the next version of the model. However, the results presented below show that the scheme is reliable and provides a realistic energy dissipation rate.

4. Calculations and results

The elevation and surface velocity potential fields are approximated in the current calculations by $M_x = 256$ and $M_y = 128$ modes in directions x and y. The corresponding grid includes $N_x \times \mathrm{N}_y = (1024 \times 512)$ knots. The vertical derivatives are approximated at vertical stretched grid $d\zeta_{j+1} = \nu d\zeta_j$, $(j = 1, 2, 3..., L_w)$ where ν =1.2and $L_w = 10$. The small number of levels used for solution of the equation for nonlinear component of the velocity potential is possible because just a surface vertical derivative for the velocity potential $\partial\Phi / \partial\zeta\left(\zeta = 0\right)$is required. The velocity potential mainly consists of an analytical component $\overline{\varphi}$,while a nonlinear component provides but small correction. To reach an accuracy of solution $\varepsilon = 10^{-6}$ for equation (11), no more than two iterations were usually sufficient.

The parameters chosen were used for solution of the problem of wave field evolution over acceptable time (of the order of 10 days). The initial conditions were assigned on the basis of empirical spectrum JONSWAP (Hasselmann et al, 1973)with a maximum placed at wave number $k_p = 100$ with angle spreading $\left(\cosh\psi\right)^{256}$.Details of initial conditions are of no importance because an initial energy level is quite low.

The total energy of wave motion $E = E_p + E_k$ (E_p - is potential energy, while E_k is kinetic energy) is calculated with the following formulas:

$$E_p = 0.25\overline{\eta^2}, \quad E_k = 0.5\overline{\overline{\left(\varphi_x^2 + \varphi_y^2 + \varphi_z^2\right)}}, \tag{25}$$

where single bar denotes averaging over the ξ and ϑ coordinates, while double bar denotes averaging over entire volume. The derivatives in (25) are calculated according to transformation (1). An equation of integral energy $E = E_p + E_k$ evolution can be represented in the following form:

$$\frac{dE}{dt} = \overline{\overline{I}} + \overline{\overline{D_b}} + \overline{\overline{D_t}} + \overline{\overline{N}}, \tag{26}$$

where $\overline{\overline{I}}$ is the integral input of energy from wind (Eqs. (13) – (15); $\overline{\overline{D_b}}$ is a rate of energy dissipation due to the wave breaking (Eqs. (21) – (24)); $\overline{\overline{D_t}}$ is a rate of energy dissipation due to33filtration of high-wave number modes ('tail dissipation', Eqs. (16) – (20)); $\overline{\overline{N}}$ is an integral effect of the nonlinear interactions described by the right-hand side of the equations when surface pressure p is equal to zero. The differential form for calculation of the energy

Ocean Sci. Discuss., https://doi.org/10.5194/os-2018-11
Manuscript under review for journal Ocean Sci.
Discussion started: 20 February 2018

transformation can be, in principle, derived from Eqs. (3) – (5), but here a more convenient and simple method was applied. Different rates of integral energy transformations can be calculated with help of fictitious time steps (i.e., apart from the basic calculations). For example, the value of $\overline{\overline{I}}$ is calculated by the following relation:

$$\overline{\overline{I}} = \frac{1}{\Delta t}\left(\overline{\overline{E^{t+\Delta t}}} - \overline{\overline{E^{t}}}\right), \tag{27}$$

where $\overline{\overline{E^{t+\Delta t}}}$ is the integral energy of wave field obtained after one time step with the right side of equation (4) containing only the surface pressure calculated with Eqs. (13) – (15). For calculation of the dissipation rate due to filtration, the right-hand side of the equations contains just the terms introduced in Eqs. (16), (17), while for calculation of the effects of breaking, only the terms introduced in (21) – (22) are in use.

An evolution of the characteristics calculated by formula (27) is shown in Fig. 2.

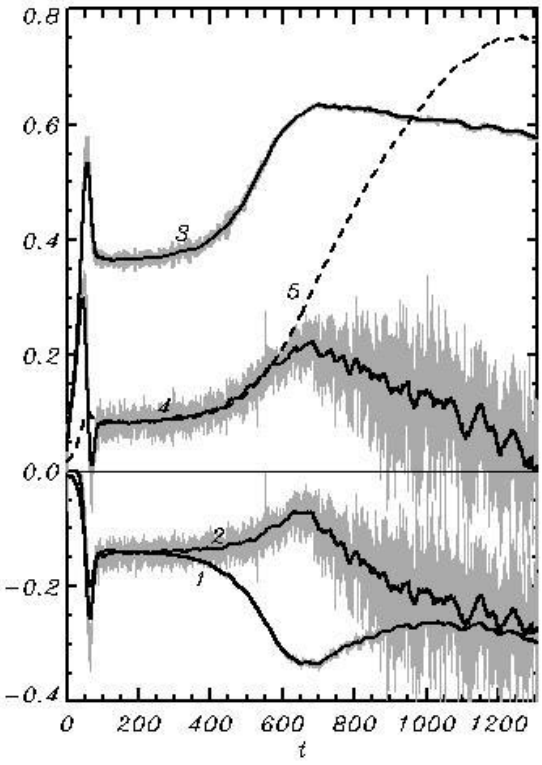

Figure 2. Evolution of integral characteristics of solution, rate of evolution of integral energy multiplied by 10^7) due to: 1 – tail dissipation D_t (Eqs. 16-20); 2 – breaking dissipation D_b (Eqs. 21-24); 3 – input of energy from wind *I* (Eqs. 13-15); 4 – balance of energy $I + D_t + D_b$. Curve 5 shows the evolution of wave energy $10^5 E$. Vertical bars of grey color show the instantaneous values; thick curve shows the smoothed behavior.

Up to the end of integration, the sum of all energy transition terms (tail dissipation $\overline{\overline{D_t}}$, breaking dissipation $\overline{\overline{D_b}}$ and energy input $\overline{\overline{I}}$) is approaching zero (curve 4), and the energy growth E (Curve 5) stops. Then the energy tends to decrease, but we are not sure about the nature of this effect. Such behavior can be explained by a fluctuating character of mutual adjustment of input

Ocean Sci. Discuss., https://doi.org/10.5194/os-2018-11
Manuscript under review for journal Ocean Sci.
Discussion started: 20 February 2018

and dissipation or simply by worsening of the approximation because of the downshifting process. Note that opposite to a more or less monotonic behavior of tail dissipation (Curve 1), the breaking dissipation is highly intermittent, which is consistent with common views on the nature of wave breaking.

The data on evolution of wave spectrum are shown in Fig. 3.

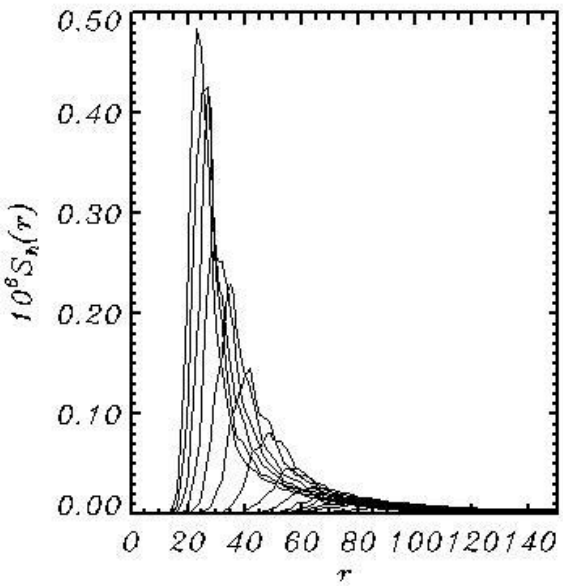

Figure 3. The wave spectra $S_h(r)$ integrated over angle ψ in the polar coordinates and averaged over consequent intervals of length about 100 units of nondimensional time *t*. The spectra are growing and shifting from right to left.

The 2-D wave spectrum $S(k,l)\left(0 \le k \le M_x, -M_y \le l \le M_y\right)$ averaged over 13 time intervals of length equal to $\Delta t \approx 100$, was transferred to the polar coordinates $S_p(\psi, r)$ $\left(-\pi/2 \le \psi \le \pi/2, 0 \le r \le M_x\right)$ and then averaged over angle ψ to obtain 1-D spectrum $S_h(r)$:

$$S_h(r) = \sum S_p(\psi, r) r \Delta\psi . \tag{28}$$

An angle $\psi = 0$ coincides with the direction of wind U, $\Delta\psi = \pi/180$.

The wave spectra $S_h(r)$ calculated by averaging over angle ψ in the polar coordinates and averaged over consequent intervals of length about 100 units of nondimensional time *t* are presented in Fig. 3. The spectra increase and move from high to low wave numbers, i.e., they undergo downshifting. A maximum value of $S_h(r)$ increases as much as 152 times. According to the data in Fig. 2, the total energy increases 44 times. This difference is explained by the spectrum narrowing and by the overlapping effect (i.e., decrease of high-frequency spectrum for long fetches). The 3-Dimages of wave spectrum $\log_{10}\left(S(k,l)\right)$ are shown in Fig. 4.

Ocean Sci. Discuss., https://doi.org/10.5194/os-2018-11
Manuscript under review for journal Ocean Sci.
Discussion started: 20 February 2018

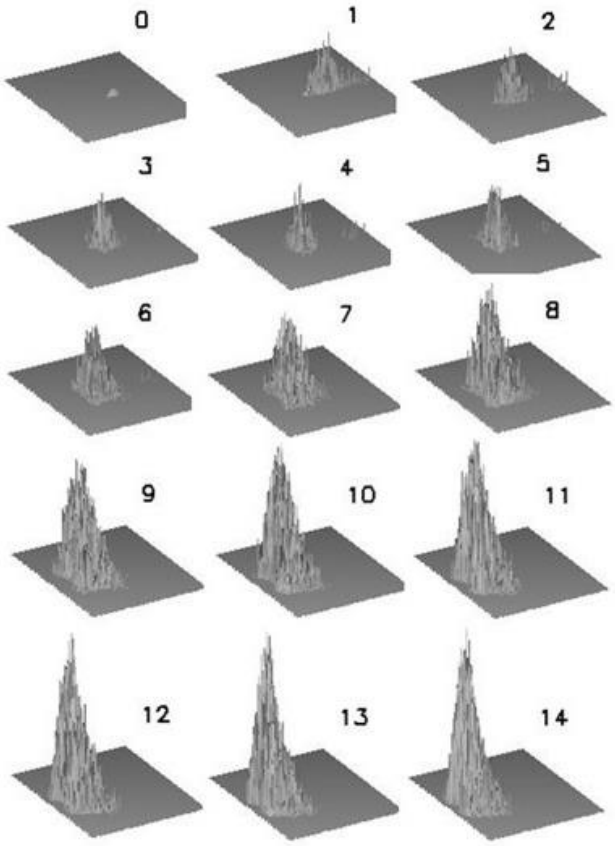

Figure 4 Sequence of 3-D images of $\lg_{10}\left(S\left(k,l\right)\right)$ where each panel corresponds to single curve in Fig. 3.
he left side refers to wave number $l\left(-M_y \le l \le M_y\right)$ and front side – to $k\left(-M \le k \le M\right)$.

As seen, each spectrum consists of separated peaks and holes[1]. This phenomenon was first observed and discussed by Chalikov et al (2014). The repeated calculations with different resolution showed that such structure of 2-D spectrum is typical. It cannot be explained by fixed combination of interacting modes, since in different runs (with the same initial conditions but different set of phases for the modes) peaks are located in different locations in Fourier space.

Another presentation is given in Fig 5where the $\log_{10}\left(S\left(\psi,r\right)\right)$, averaged over the successive seven period length $\Delta t = 200$, is given. The first panel with a mark 0 refers to initial conditions. Disturbances within the range $(125 < k < 150)$ reflect initial adjustment of the input and dissipation at high wave number slope of spectrum. The pictures characterize well the downshifting and angle spreading of spectrum due to nonlinear interactions.

Evolution of the integrated over angles ψ wave spectrum $S_h\left(r\right)$ can be described with the equation

[1]The wave spectrum looks rather like La Sagrada Familia (Gaudi) in Barcelona than the St. Mary Axe ('Pickle') in London.

Ocean Sci. Discuss., https://doi.org/10.5194/os-2018-11
Manuscript under review for journal Ocean Sci.
Discussion started: 20 February 2018

$$\frac{dS_h(r)}{dt} = I(r) + D_t(r) + D_b(r) + N(r), \tag{29}$$

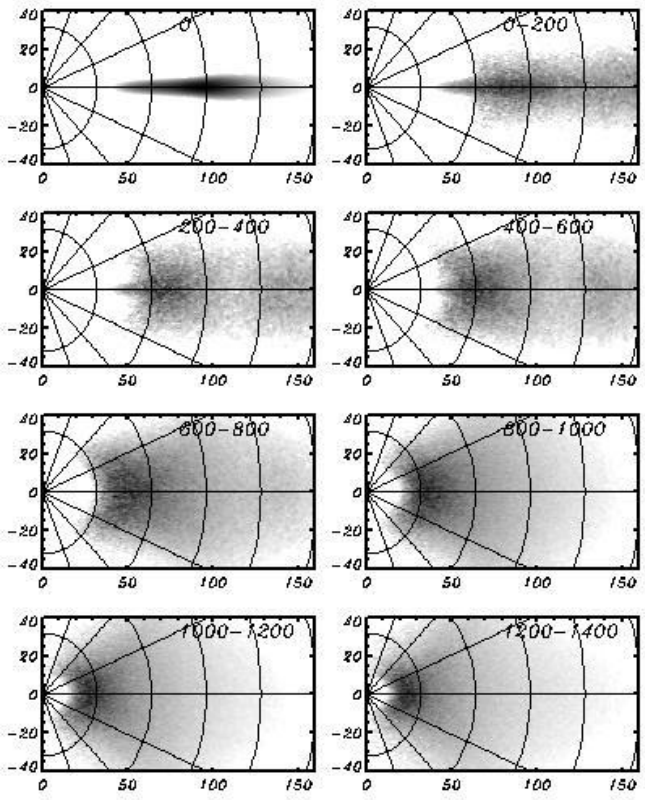

Figure 5. Sequence of 2-D images of $\lg_{10}(S(k,l))$ averaged over consequent seven periods length $\Delta t = 200$. Numbers indicate the period of averaging (first panel marked 0, refers to initial conditions). Horizontal and vertical axes correspond to wave numbers k and l correspondingly

where $I(r), D_t(r), D_b(r)$ and $N(r)$ are the spectra of the input energy, tail dissipation, breaking dissipation and a rate of nonlinear interactions, all obtained by integration over angles ψ. All of the spectra shown below were obtained by transformation of 2-D spectra into the polar coordinate (ψ, r) and then integrated over angles ψ within the interval $(-\pi/2, \pi/2)$. The spectra can be calculated using an algorithm similar to the algorithm (27) for integral characteristics. For example, the spectrum of energy input $I(k,l)$ is calculated as follows:

$$I(k,l) = \left(S_c^{t+\Delta t}(k,l) - S_c^t(k,l)\right)/\Delta t, \tag{30}$$

where $S_c(k_x, k_y)$ is a spectrum of columnar energy calculated by relation

$$S_c(k,l) = \frac{1}{2}\left(h_{k,l}^2 + h_{-k,-l}^2 + \int_{-H}^{0}\left(u_{k,l}^2 + u_{-k,-l}^2 + v_{k,l}^2 + v_{-k,-l}^2 + w_{k,l}^2 + w_{-k,-l}^2\right)d\zeta\right) \tag{31}$$

where grid values of velocity components u, v, w are calculated by relations:

$$u = \varphi_\xi + \varphi_\zeta \eta_\xi, \quad v = \varphi_\vartheta + \varphi_\zeta \eta_\vartheta, \quad w = \varphi_\zeta, \tag{32}$$

and $u_{k,l}, v_{k,l}$ and $w_{k,l}$ are their Fourier coefficients.

Ocean Sci. Discuss., https://doi.org/10.5194/os-2018-11
Manuscript under review for journal Ocean Sci.
Discussion started: 20 February 2018

For calculation of $I(k_x, k_y)$ the fictitious time steps Δt are made only with a term responsible for the energy input, i.e., surface pressure p. Spectrum $I(k,l)$ was averaged over the periods $\Delta t \approx 100$, then transformed into a polar coordinate system and integrated in Fourier space over angles ψ within the interval $(-\pi/2, \pi/2)$.

The evolution of input spectra (Fig. 6) is, in general, similar to that of wave spectra shown in Fig. 3. Note that a maximum of spectra is located at the maximum of wave spectra since the input depends mainly on spectral density, while the dependence on frequency is less important.

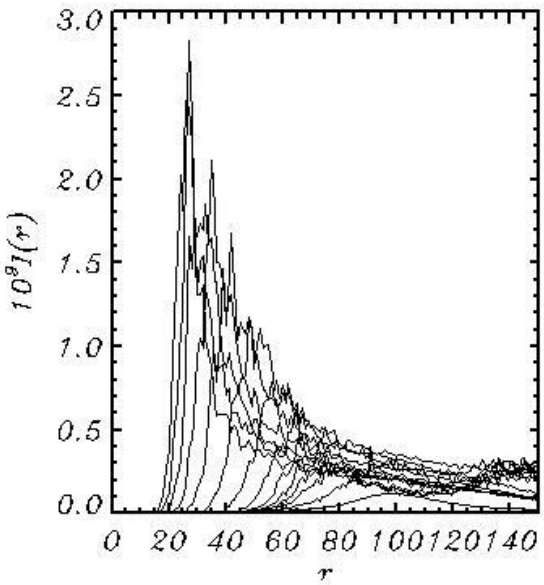

Figure 6. The spectrum of energy input $I(r)$ integrated over angle ψ in the polar coordinates and averaged over consequent intervals of length about 100 units of nondimensional time *t*.

Algorithm (29) – (32) was applied for calculation of the dissipation spectra due to dumping of a high-wave number part of spectrum (tail dissipation) and for calculation of the spectrum of breaking dissipation. In the first case, the fictitious time step was made taking into account the terms described by Eqs (16) – (20), while in the second case the time step was made using the terms described by Eqs (21) – (24).

The spectra of tail dissipation calculated similar to spectra $I(r)$ are shown in Fig. 7.Dissipation occurs at the periphery of spectrum, outside the ellipse with semi-axes $d_m M_x$ and $d_m M_y$ [2].This is why such dissipation, averaged over angles, seems to affect a middle part of 1-D spectrum. The tail dissipation effectively stabilizes the solution.

The breaking dissipation averaged over angles is presented in Fig. 8.As seen, the breaking dissipation has a maximum at spectral peak. It does not mean that in the vicinity of wave peak the probability of large curvilinearity is quite high. The high rate of breaking dissipation can be explained by high wave energy in the vicinity of wave peak. The energy lost

[2]The 2-D Fourier spectral ‘tail’ looks like ‘peacock’ tail.

Ocean Sci. Discuss., https://doi.org/10.5194/os-2018-11
Manuscript under review for journal Ocean Sci.
Discussion started: 20 February 2018

through breaking, described by the diffusion mechanism, correlates with the energy of breaking waves. Opposite to high wave number dissipation which regulates shape of spectral tail, the breaking dissipation forms the main energy-containing part of spectrum.

The diffusion mechanism suggested in (21), (22) modifies an elevation and surface stream function in a close vicinity of breaking point. The amplitudes of side perturbation are small and decrease very quickly over the distance from a breaking point.

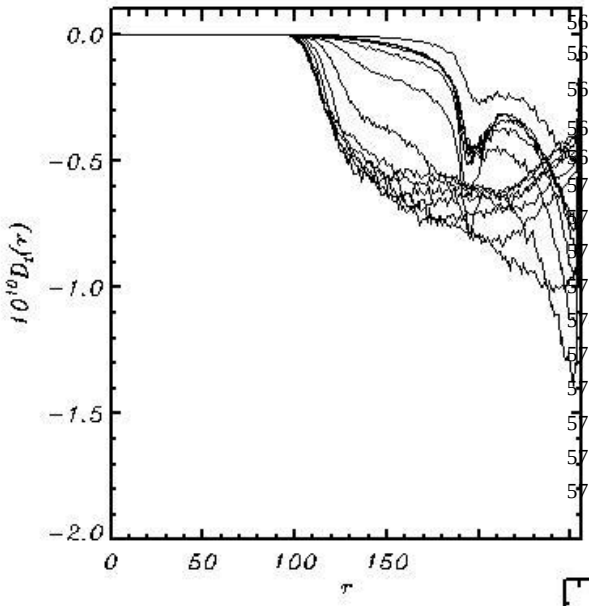

Figure 7. Tail dissipation spectra $D_t(r)$ integrated over angle ψ in the polar coordinates and averaged over consequent intervals of length about 100 units of nondimensional time *t*.

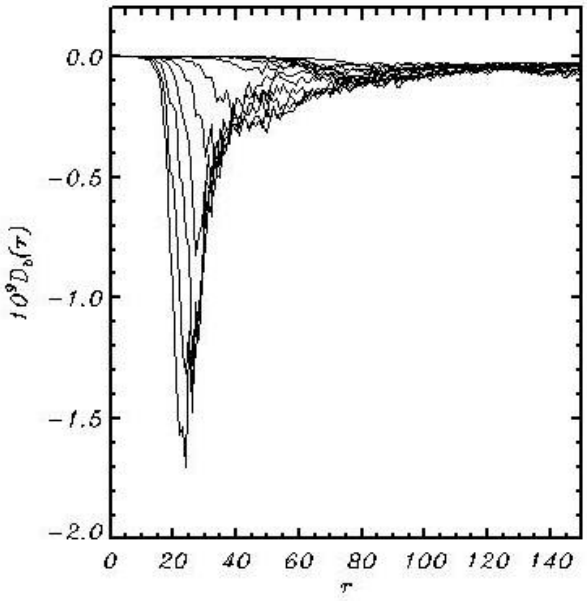

Figure 8, Breaking dissipation spectra $D_b(r)$ integrated over angle ψ in the polar coordinates and averaged over consequent intervals of length about 100 units of nondimensional time *t*.

Ocean Sci. Discuss., https://doi.org/10.5194/os-2018-11
Manuscript under review for journal Ocean Sci.
Discussion started: 20 February 2018

An example of profile of the energy input due to breaking $D_b(x)$ is given in Fig. 9. As seen, energy input is fluctuating around the breaking point. A diffusion operator chosen for breaking parameterization not only decreases total energy but also redistributes the energy between Fourier modes in Fourier space.

In general, for the specific conditions considered in the paper, the breaking is an occasional process taking place in a small part of domain. The kurtosis of input energy due to the breaking $D_b(\xi,\vartheta)$, i.e., the value

$$Ku = \overline{\overline{D_b^4}}\left(\overline{\overline{D_b^2}}\right)^{-2} - 3 \tag{33}$$

is of the order of 10^3, which corresponds to plain function with occasional separated peaks.

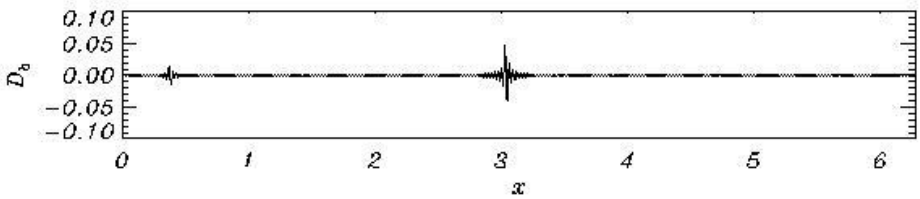

Figure 9. Example of energy input due to breaking $D_b(x)$.

The number of breaking points in terms of percentage of the total number of points is given in Fig. 10. As seen, the number of breaking events is going down to $t = 600$ and then is growing up to the end of the calculations. The number of breaking events is not directly connected with intensity of breaking, which is seen when comparing Fig. 10 and curve 2 in Fig.1.

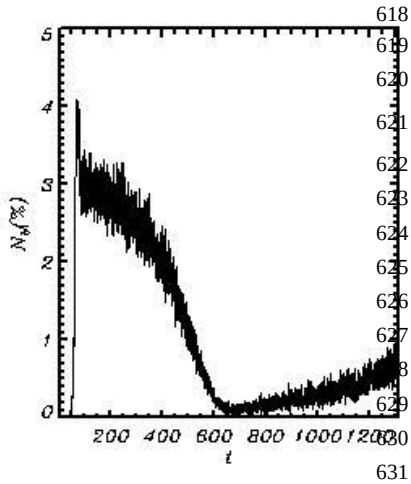

Figure 10. Evolution of number of wave breaking events N_b expressed in percentage of the number of grid points $N_x \times N_y$.

An integral term describing nonlinear interaction $\overline{\overline{N}}$ in Eq. (26) is small, but the magnitude of spectrum $N(r)$ is comparable with input $I(r)$ and dissipation $D_t(r)$ and $D_b(r)$ terms. The presentation of term $N(r)$ in a form shown in Figs. (6) – (8) is not clear. This is why the spectra

Ocean Sci. Discuss., https://doi.org/10.5194/os-2018-11
Manuscript under review for journal Ocean Sci.
Discussion started: 20 February 2018

$10^8 N(r)$ averaged over interval $\Delta t = 100$ are plotted separately in Fig. 11 for the last eight intervals (thick curves) together with the wave spectrum $10^6 S_h(r)$. In general, the shapes of spectrum $N(r)$ agree with the conclusions of the quasi-linear Hasselmann (1962) theory. At low wave number slope of spectrum the nonlinear influx of energy is positive while at the opposite slope it is negative. This process produces shifting of spectrum to the lower wave number (downshifting). Opposite to the Hasselmann's theory, these results are obtained by solution of full three-dimensional equations. It would be interesting to compare our results with the calculations of Hasselmann's integral. Unfortunately, neither of the existing programs of such type permits

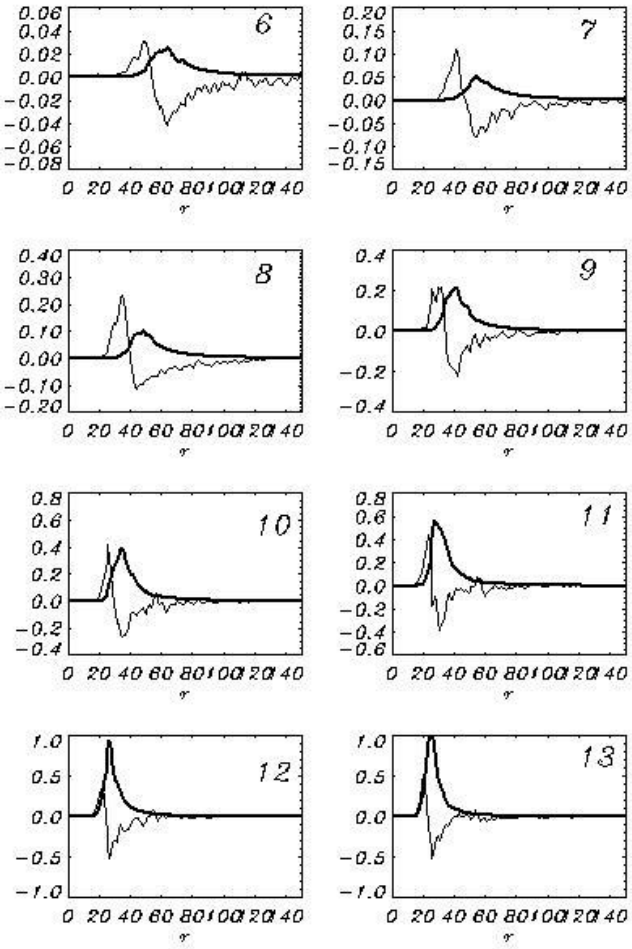

Figure 11. Sequence of wave spectra $S_h(r)$ (thick curves) and nonlinear input term $N(r)$ (thin curves) averaged over consequent eight periods of length $\Delta t = 100$ starting from 6th period.

doing calculations with such a high resolution that was used in the current model. Note that nonlinear interactions also produce widening of spectrum.

Obviously, the nonlinearity is quite an important property of surface waves. The contribution of nonlinearity can be estimated, for example, by comparison of the kinetic energy

Ocean Sci. Discuss., https://doi.org/10.5194/os-2018-11
Manuscript under review for journal Ocean Sci.
Discussion started: 20 February 2018

of linear component $E_l = 0.5\overline{\overline{\left(\bar{\varphi}_x^2 + \bar{\varphi}_y^2 + \bar{\varphi}_z^2\right)}}$ and the total kinetic energy E_k (Fig. 12). A ratio E_l / E_k as a function of time remains very close to 1, which proves that the nonlinear part of energy makes up just a small percentage of the total energy. It does not mean that the role of nonlinearity is small; its influence can manifest itself over large time scales.

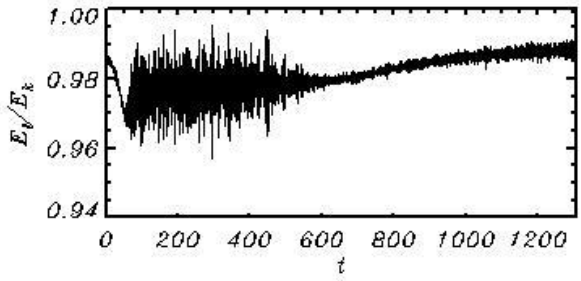

Figure 12. Time evolution of ratio E_l / E_k .

The time evolution of integral spectral characteristics is presented in Fig. 13.

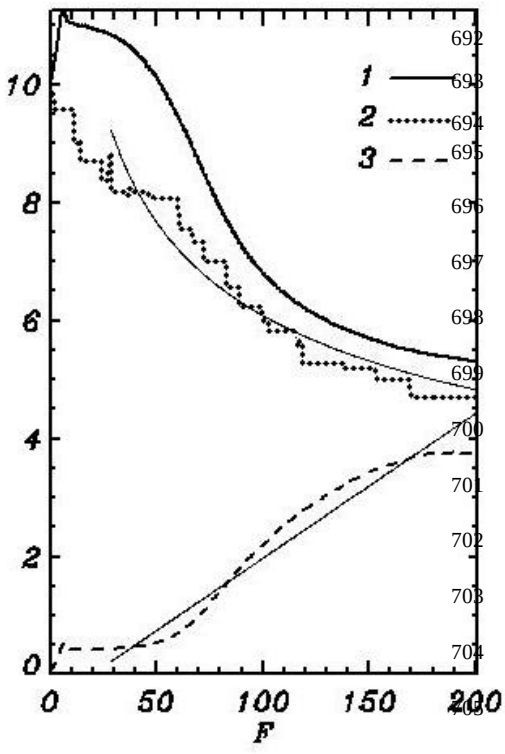

Figure 13. Time evolution of: weighted frequency ω_w (1) (Eq. 34); spectral peak frequency ω_p (2); full energy E (3) (Eq. 25). Thin curves are empirical 97distance passed by the spectral peak.

Curve 1 corresponds to the weighted frequency ω_p

Ocean Sci. Discuss., https://doi.org/10.5194/os-2018-11
Manuscript under review for journal Ocean Sci.
Discussion started: 20 February 2018

$$\omega_p = \left(\frac{\int kSdkdl}{\int Sdkdl} \right)^{1/2}, \tag{34}$$

where integrals are taken over the entire Fourier-domain. The value k_w is not sensitive to the details of spectrum, hence, it well characterizes the position of spectrum and its shifting. Curve2 describes evolution of the spectral maximum. The step shape of curve corresponds to the fundamental property of downshifting. Opposite to the common views, development of spectrum occurs not monotonically, but by appearance of a new maximum at lower wave number as well as by attenuation of the previous maximum. Curve 3 describes the change of total energy $E = E_p + E_k$. As seen all three curves have a tendency for saturation (decrease of evolution rate).

The numerical experiment reproduces the case when development of wave field occurs under the action of permanent and uniform wind. This case corresponds to JONSWAP experiment. Despite large scatter, the data allow us to construct empirical approximations of wave spectrum, as well as to investigate the evolution of spectrum as a function of fetch F. In particular, it is suggested that the frequency of spectral peak changes as $F^{-1/3}$,while full energy grows linearly with F. Neither of the dependences can be exact, since they do not take into account the approaching to a stationary regime. Besides, the dependence of frequency on fetch is singular at $F = 0$.

The value of fetch in periodic problem can be calculated by integration of peak phase velocity $c_p = |k|^{-1/2}$ over time.

$$F = \int_{t_0}^{t} c_p dt \tag{35}$$

The JONSWAP dependencies for the wave number of spectral peak k_p and full energy E are shown in Fig 13 by thin curves. Dependence $\omega_p \square F^{1/3}$ is qualitatively valid. Dependence of the total energy on fetch does not look like a linear one, but it is worth to note that JONSWAP dependence is evidently inapplicable to a very small and large fetch.

5. Discussion

A model based on the full three-dimensional equations potential motion with free surface was used for simulation of development of wave fields. The model is written in the surface-following nonstationary non-orthogonal coordinate system. The details of numerical scheme and the results of validation of the model were described in (Chalikov et al, 2014). The main difference between the given model and HOS model (Ducroset et al, 2017) is that our model is based on direct solution of 3-D equations for velocity potential. This approach is similar to that developed at Technical University of Denmark (TUD, see Engsig-Karup et al, 2009). Actually, the models developed at TUD are directed to solution of a variety of problems including such problems as modeling of wave interaction with submerged objects and simulation of wave regime in the basins with real shape and topography.

In the current paper a three-dimensional model was used for simulation of development of wave field under the action of wind and dissipation. The input energy is described by single

Ocean Sci. Discuss., https://doi.org/10.5194/os-2018-11
Manuscript under review for journal Ocean Sci.
Discussion started: 20 February 2018

term, i.e., surface pressure p in Eq. (4). It is traditionally assumed that the complex pressure amplitude in Fourier space is linearly connected with the complex elevation amplitude with a complex coefficient called β – function. Such simple formulations can be imperfect. Firstly, it is assumed that wave field is represented by superposition of linear modes with slowly changing amplitudes and phase velocity obeying the linear dispersive relation. This assumption is valid only for a low-frequency part of spectrum. In reality, the amplitudes of medium and high-frequency modes undergo fluctuations created by reversible interactions. A solid dispersion relation does not connect their phase velocities with wave number. Besides, it is also quite possible that the suggestion of linearity of the connection between pressure and elevation amplitudes is not precise, i.e., β – function can depend on amplitudes of modes.

We are not familiar with any observation data that can be used for formulation of a more sophisticated scheme for calculation of the input energy to waves. The only method that can give more or less reliable results is mathematical modeling of the statistical structure of turbulent boundary layer above a curvilinear moving surface, which characteristics satisfy kinematic conditions. As a whole, the problem of boundary layer seems even more complicated than the wave problem itself. Some early attempts to solve this problem were made on the basis of the finite difference two-dimensional model of boundary layer written in the simple surface following coordinate (see review Chalikov, 1986). Waves were assigned as a superposition of linear modes with random phases corresponding to the empirical wave spectrum. This approach was quite accurate since it did not take into consideration the nonlinear properties of surface (for example, the sharpness of real waves and the absence of dispersive relation for waves of medium and high frequencies. The next step was formulation of coupled models for boundary layer and potential waves, both written in the conformal coordinates (Chalikov, Rainchik, 2014). The calculations showed that pressure field consists mostly of random fluctuations not directly connected with waves. A small part of these fluctuations is in phase with surface disturbances. The calculated values of β in Eq. (13) have large dispersion. However, since the volume of data was very large, the shape of β-function was found with high-level accuracy. Probably, approximation of β used in the current work can be considered as most adequate. We are planning additional investigations based on coupled wind-wave models. The next step in investigations of Wave boundary Layer (WBL)should use a three-dimensional LES approach. Note that even availability of large volume of data on the structure of WBL does not make the problem of parameterization of wind input in spectral wave models easily solvable, since the pressure is characterized by a broad continuous spectrum created by nonlinearity.

The wave breaking is obviously even more complicated than the input energy. Nevertheless, this problem can be simplified, if common ideas used in the numerical fluid mechanics are accepted. For example, in LES modeling the more or less artificial viscosity is introduced to prevent too large local velocity gradients. It is a fact that the numerical instability terminating computations precedes wave breaking. Hence, the scheme should prevent breaking approach to preserve stability of the numerical scheme. Hence, a wave model should contain the algorithms preventing appearance of too large slopes. The criterion of breaking is introduced not for recognizing of the breaking itself, but for the choice of places where it might happen (or, unfortunately, might not happen). Finally, the algorithm should produce local smoothing of elevation (and surface potential). The algorithm should be highly selective so that 'breaking' would occur within narrow intervals and not affect the entire area. The exact criteria of breaking events (most evident of them is the breaking itself) cannot be used for parameterization of

breaking since in coordinate system (1) the numerical instability occurs long before breaking. In our opinion, the most sensitive parameter indicating potential instability is the curvilinearity (second derivative) of elevation.

In the current work, the breaking is parameterized by diffusion algorithm with the nonlinear coefficient diffusion providing high selectivity of smoothing. We admit that such approach can be realized in many different forms. The same situation is observed in a problem of turbulence modeling for parameterization of subgrid scales.

We can finally conclude that the physics included in the wave model is still based on a shaky ground. Nevertheless, the result of the calculations looks quite realistic, which convinces us that the approach deserves further development.

The numerical models of waves similar to that considered in the paper have a lot of important applications. Firstly, they are a perfect tool for development of physical parameterizations schemes in spectral wave models. Secondly, the direct model can be used in future for numerical simulation of wave processes in the basins of small and medium size. These investigations can be based on HOS model (Ducroset et al, 216) or the model used in the current paper. However, the most universal approach seems to be developed at the Technical University of Denmark (see Engsig-Karup, 2009). Any model used for a long-term simulation of wave field evolution should include the algorithms describing transformation of energy, similar to those considered in the current paper.

Acknowledgements

The authors thank Mrs. O. Chalikova for her assistance in preparation of the manuscript. The investigation is supported by Russian Science Foundation, Project 16-17-00124.

References

Babanin, A.V., 2011. Breaking and Dissipation of Ocean Surface Waves. Cambridge University Press, 480p

Chalikov D.V. 1978. Numerical simulation of wind-wave interaction. J. Fluid. Mech. 87, 561-582

Chalikov, D.V.: Numerical simulation of the boundary layer above waves. Bound. Layer Met., 34. 63-98 1986

Chalikov, D.: The Parameterization of the Wave Boundary Layer. J. Phys. Oceanogr., 25, 1335-1349, 1995

Chalikov, D.: Statistical properties of nonlinear one-dimensional wave fields. Nonlinear processes in geophysics. 12, 1-19, 2005

Chalikov, D.: Freak waves: their occurrence and probability. Phys of Fluid, 21, 076602, 2009

Chalikov, D.: Numerical modeling of sea waves, Springer, DOI 10.1007/978-3-319-32916-1, 330 pp. 2016

Chalikov, D. and Makin, V.: Models of the wave boundary layer. Bound. Layer Met., 56, 83-99, 1991

Chalikov, D. and Belevich, M.: One-dimensional theory of the wave boundary layer. Bound. Layer Met., 63, 65-96, 1992

Chalikov D. and Sheinin, D.: Direct Modeling of One-dimensional Nonlinear Potential Waves. Nonlinear Ocean Waves, ed. W. Perrie, Advances in Fluid Mechanics, 17, 207- 258, 1998

Chalikov D., Babanin AV and Sanina, E.: Numerical Modeling of Three-Dimensional Fully Nonlinear Potential Periodic Waves. Ocean dynamics. 64, 10, 1469-1486, 2014

Chalikov, D. and Rainchik, S.: Coupled Numerical Modelling of Wind and Waves and the Theory of the Wave Boundary Layer. Boundary-Layer Meteorol. 138:1–41. DOI 10.1007/s10546-010-9543-7, 2010

Chalikov, D. and Babanin, A. V.,: Simulation of Wave Breaking in One-Dimensional Spectral Environment. Journal Phys. Ocean., Vol. 42, No. 11, 1745-1761, 2012

Chalikov D. and Babanin A.V.: Simulation of one-dimensional evolution of wind waves in a deep water. Physics of fluid, 26 (9), 096607, 2014

Chalikov D. and Babanin A.V.: Nonlinear sharpening during superposition of surface waves. Ocean Dynamics. 66(8), 931-937, 2016a

Chalikov D. and Babanin A.V.: Comparison of linear and nonlinear extreme wave statistics. Acta Oceanologica Cinica. 35,5,99-105, DOI:10,1007/313131-016-0862-5, 2016b

Donelan, M.A., Babanin A.V. Young I.R., Banner, M.L., and McCormick, C.: Wave follower field measurements of the wind input spectral function. Part I. Measurements and calibrations. J. Atmos. Oceanic tech. 22, 799-813, 2005

Donelan, M.A., Babanin A.V. Young I.R. and Banner, M.L.: Wave follower field measurements of the wind input spectral function. Part II. Parameterization of the wind input. J. Phys. Oceanogr. 36, 1672-1688, 2006

Ducrozet G., Bonnefoy F., Le Touzé D. and Ferrant P.: HOS-ocean: Open-source solver for nonlinear waves in open ocean based on High-Order Spectral method. Comp. Phys. Comm., doi:10.1016/j.cpc.2016.02.017, 2016

Engsig-Karup A.P., Harry B., Bingham H.B. and Lindberg O.: An efficient flexible-order model for 3D nonlinear water waves. J. Comput. Physics 228(6), 2100-2118, 2009

Hasselmann, K.: On the non-linear energy transfer in a gravity wave spectrum, Part 1, . J. Fluid Mech., 12, 481–500, 1962

Hasselmann K, Barnett RP, and Bouws E. et al.: Measurements of wind-wave growth and swell decay during the Joint Sea Wave Project (JONSWAP). Tsch. Hydrogh. Z. Suppl. 1973, A8(12), 1-95, 1973

Hasselmann, D., and J. Bösenberg,: Field measurements of wave-induced pressure over wind-sea and swell. J. Fluid Mech., **230,** 391–428, 1991

Hsiao, S. V., and O. H. Shemdin,: Measurements of wind velocity and pressure with a wave follower during MARSEN. J. Geophys. Res., 88**,** 9841–9849, 1983

Iafrati A.: Numerical Study of the Effects of the Breaking Intensity on Wave Breaking Flows. J Fluid Mech,, 622, pp 371-411, 2009

Miles, J.W. 1957: On the generation of surface waves by shear flows. J. Fluid Mech,3, 02, doi: 10.1017/S0022112057000567, 1957

Rogers, W.E., Babanin, A.V. and Wang, D.W.: Observation-consistent input and whitecapping-dissipation in a model for wind-generated surface waves: Description and simple calculations. J. Atmos. Oceanic Tech., 29(9), 1329-1346, 2012

Snyder, R. L., Dobson, F.W., Elliott, J.A., and Long, R.B.: Array measurements of atmospheric pressure fluctuations above surface gravity waves. J. Fluid Mech., 102**,** 1–59, 1981

Ting C.-H, Babanin, A.V., Chalikov, D. and Tai-Wen Hsu,: Dependence of drag coefficient on the directional spreading of ocean waves, J. Geophys. Res., 117, C00J14, doi:10.1029/2012JC007920, 2012

Tolman H. and D. Chalikov 1996: On the source terms in a third-generation wind wave model. Journ. Phys. Oceanogr. 1996, 26, 2497-2518, 1996

Tolman H.,L and the WAVEWATCH III °R Development Group: User manual and system documentation of WAVEWATCH III °R version 4.18 Environmental Modeling Center Marine Modeling and Analysis Branch, Contribution No. 316, 2014

Figure captions

Figure 1. Probability of curvilinearity $\eta_{\xi\xi}$. Thick curve calculated with full 3-D model; thin curve is a normal probability.

Figure 2. Evolution of integral characteristics of solution, rate of evolution of integral energy multiplied by 10^7) due to: 1 – tail dissipation D_t (Eqs. 16-20); 2 – breaking dissipation D_b (Eqs. 21-24); 3 – input of energy from wind *I* (Eqs. 13-15); 4 – balance of energy $I + D_t + D_b$. Curve 5 shows the evolution of wave energy $10^5 E$. Vertical bars of grey color show the instantaneous values; thick curve shows the smoothed behavior.

Figure 3. The wave spectra $S_h(r)$ integrated over angle ψ in the polar coordinates and averaged over consequent intervals of length about 100 units of nondimensional time *t*. The spectra are growing and shifting from right to left.

Figure 4 Sequence of 3-D images of $\lg_{10}(S(k,l))$ where each panel corresponds to single curve in Fig. 3. The left side refers to wave number $l(-M_y \le l \le M_y)$ and front side – to $k(0 \le k \le M_x)$

Figure 5. Sequence of 2-D images of $\lg_{10}(S(k,l))$ averaged over consequent seven periods length $\Delta t = 200$. Numbers indicate the period of averaging (first panel marked 0, refers to initial conditions). Horizontal and vertical axes correspond to wave numbers *k* and *l* correspondingly

Figure 6. The spectrum of energy input $I(r)$ integrated over angle ψ in the polar coordinates and averaged over consequent intervals of length about 100 units of nondimensional time *t*.

Figure 7. Tail dissipation spectra $D_t(r)$ integrated over angle ψ in the polar coordinates and averaged over consequent intervals of length about 100 units of nondimensional time *t*.

Figure 8, Breaking dissipation spectra $D_b(r)$ integrated over angle ψ in the polar coordinates and averaged over consequent intervals of length about 100 units of nondimensional time *t*.

Figure 9. Example of energy input due to breaking $D_b(x)$.

Figure 10. Evolution of number of wave breaking events N_b expressed in percentage of the number of grid points $N_x \times N_y$.

Figure 11. Sequence of wave spectra $S_h(r)$ (thick curves) and nonlinear input term $I(r)$ (thin curves) averaged over consequent eight periods of length $\Delta t = 100$ starting from 6th period.

Figure 12. Time evolution of ratio E_l / E_k .

Figure 13. Time evolution of: weighted frequency ω_w (1) (Eq. 34); spectral peak frequency ω_p (2); full energy E (3) (Eq. 25). Thin curves are empirical dependence for peak wave number and energy. F is a distance passed by the spectral peak.